# Multicomponent Diffusion and Time Evolution

A Major Qualifying Project (MQP) Report
Submitted to the Faculty of
WORCESTER POLYTECHNIC INSTITUTE
in partial fulfillment of the requirements
for the Degree of Bachelor of Science in

Physics,
Electrical and Computer Engineering

By:

Katherine Hudek

Project Advisor:

Professor L. Ramdas Ram-Mohan

Date: April 2021

## Abstract

Multicomponent diffusion and the time evolution of component concentrations are analyzed mathematically and equations presented which describe the behavior both with and without the need for the traditional interdiffusion coefficients. Both approaches were simulated and predicted results for time-evolved concentrations from a known starting state were compared to the results from a prior physical experiment involving the diffusion of three metals. The results for both approaches generally agree with the experimental results. The new approach bypassing the need for calculating the interdiffusion coefficients appears viable.

## Contents



## List of Tables



## List of Figures

# 1 Introduction

At a high level, the topic of diffusion is concerned with the net movement of one or more items of interest from one region to another over time. This core concept plays an important role in a wide range of disciplines in the sciences, engineering, and beyond, such as electrical engineering, physics, chemistry, biology, pharmaceuticals, sociology, and economics. For example, the semiconductor and electronics industry depends on a firm understanding of the diffusion behavior of atoms of different elements used in the design, manufacture, and use of semiconductor components and metallic interconnects.

In general terms, components will tend to flow from areas of higher concentration to those of lower concentrations (flux will be proportional to the negative of the concentration gradient). In the simplest case, one is concerned with the diffusion of a single component, such as a single metal. The behavior over space and time can be characterized with a set of differential equations involving concentration ($C(x,t)$), flux ($J(x,t)$), and a diffusion coefficient ($D$). This area has been studied extensively and the behavior is governed by a set of equations described in section 2.1. The solution to the concentration is known in terms of a standard function known as $\text{erf}(x)$.

The situation becomes more intricate in a multicomponent situation with multiple components all influencing each others' diffusion and the behavior becomes more complex. Section 2.2 describes the modifications to the key equations to extend the single component case to multiple components. The current approach expands the single component concept of a diffusion coefficient $D$ to a set of interdiffusion coefficients $D_{ij}$ between the different components. The focus of this report will be the multicomponent case in a single dimension of space. The specific case used as an example will be that of interdiffusion between three metals (Copper, Nickel, Zinc), for which physical experiments have been performed at Purdue University [14] [5].

The theoretical basis for determining interdiffusion coefficients from a set of experi-

mental data is given in Section 3. Finite element methods are used to estimate the spatial derivative of concentrations at element nodes at a give time by performing a best fit of cubic Hermite interpolation polynomials to the data as developed by Ram-Mohan, and then a method of moments first developed by Dayananda is used to generate sufficient equations to solve for interdiffusion coefficient values. The interdiffusion coefficients vary with concentration, but in small element regions they are treated as an average constant value. Simulations were performed to apply this approach to a set of experimental data with results described in Section 4.

Section 5 describes the theoretical basis and derivation of an equation to time-evolve a system and predict the future concentration profiles of multiple components given their known concentrations at an initial time along with their interdiffusion coefficients (determined earlier). Simulations were performed to apply this approach, with results described in Section 6.

The ability to time evolve a system and predict future concentrations without first determining interdiffusion coefficients is desirable, and the theoretical basis for the new approach that may be able to accomplish this is described in Section 7.1. Simulations were performed to apply this approach, with results described in Section 7.2.

The two different approaches are illustrated in Figure 1.

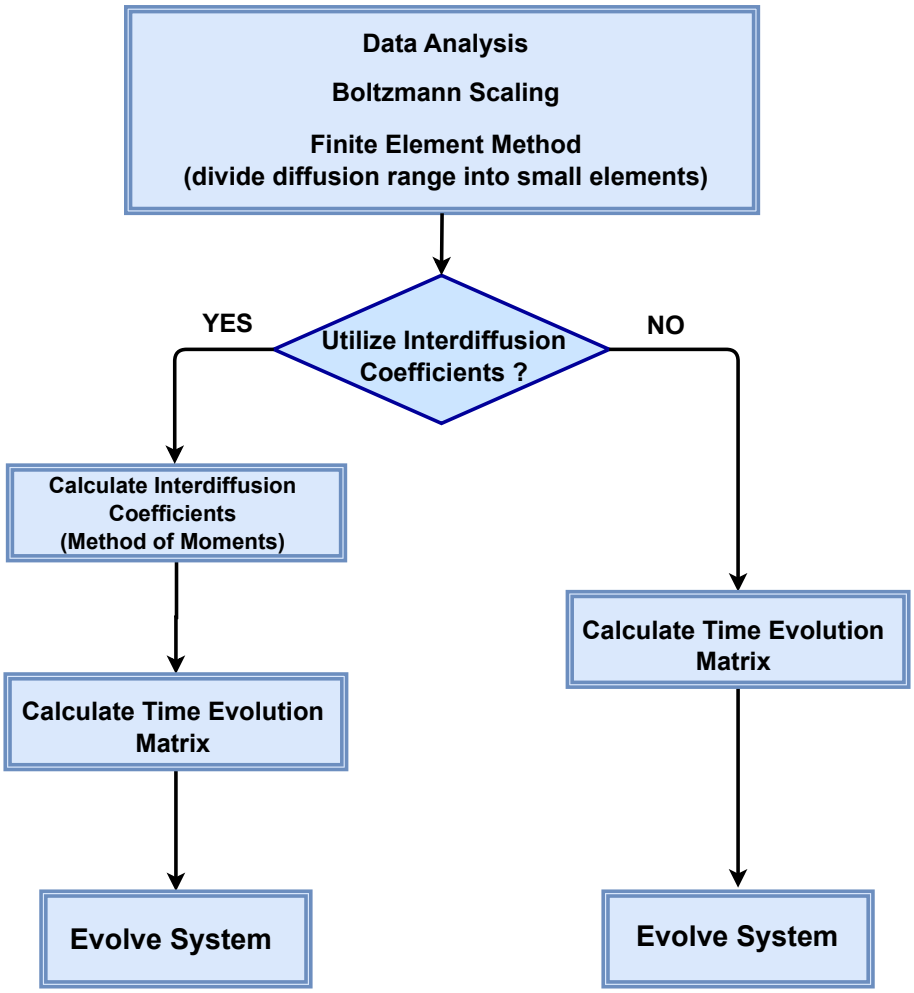


Figure 1: Approach with and without calculating interdiffusion coefficients are shown.

## 2 Diffusion Theory and Background

### 2.1 Single Component One Dimensional Diffusion

For the case of one component, the flux $J$ is driven by the change in concentration $C$ as shown in Eq. 1, known as Fick's Law (or Fick's First Law) [1].

$$J(x,t) = -D\frac{\partial C(x,t)}{\partial x}, \tag{1}$$

Note that both $J$ and $C$ are functions of both space, $x$, and time, $t$. The variable $D$ is the diffusion coefficient and relates the flux to the rate of change in concentration with respect to space. Eq. 2 is known as the Equation of Continuity and relates the rate of change in flux with respect to space to the rate of change in concentration with respect to time.

$$\frac{\partial J}{\partial x} + \frac{\partial C}{\partial t} = 0. \tag{2}$$

Combining Eq. 2 with 1 leads to Eq. 3, known as the Diffusion Equation, or Fick's Second Law, for one component in one dimension.

$$\frac{\partial C(x,t)}{\partial t} = \frac{\partial}{\partial x}\left(D\frac{\partial C(x,t)}{\partial x}\right). \tag{3}$$

This is a differential equation involving partial derivatives with respect to position ($x$) and time ($t$).

For an example one dimensional case with $x$ ranging from $x_L$ on the left to $x_R$ on the right, the solution for concentration is

$$C(x,t) = \frac{C(x_L)}{2}\left(1 - \text{erf}\left(\frac{x}{2\sqrt{Dt}}\right)\right), \tag{4}$$

where erf() is the function defined by

$$\mathrm{erf}(x) = \frac{2}{\sqrt{\pi}} \int_0^x \exp(-\alpha^2) d\alpha. \tag{5}$$

The diffusion equation can be simplified with a change of variable suggested by Boltzman [2] to substitute for the $x/\sqrt{t}$ term. Utilizing $\lambda$ as defined in Eq. 6

$$\lambda = x/\sqrt{t}, \tag{6}$$

where

$$\left.\frac{\partial}{\partial t}\right|_x = \frac{\partial \lambda}{\partial t}\frac{\partial}{\partial \lambda} = \frac{-x}{2t^{\frac{3}{2}}}\frac{\partial}{\partial \lambda}, \tag{7}$$

$$\left.\frac{\partial}{\partial x}\right|_t = \frac{\partial \lambda}{\partial x}\frac{\partial}{\partial \lambda} = \frac{1}{\sqrt{t}}\frac{\partial}{\partial \lambda}, \tag{8}$$

and inserting into Eq. 3, one obtains

$$\frac{-x}{2t^{\frac{3}{2}}}\frac{dC}{d\lambda} = \frac{1}{\sqrt{t}}\frac{d}{d\lambda}\left(D(C)\frac{1}{\sqrt{t}}\frac{dC}{d\lambda}\right), \tag{9}$$

where the diffusion coefficient is more accurately represented as a function of the concentration, $D(C(x,t))$. Combining terms and substituting for $x$ with $\lambda\sqrt{t}$ yields

$$\frac{-\lambda}{2}\frac{dC}{d\lambda} = \frac{d}{d\lambda}\left(D(C)\frac{dC}{d\lambda}\right), \tag{10}$$

a simpler differential equation with respect to the variable $\lambda$.

#### 2.1.1 Experimentally Determining Single Component One Dimension Diffusion Coefficients

As mentioned earlier, the diffusion coefficient $D$ is actually a function of the concentration, $D(C)$, and the concentration is itself a function of space and time, $C(x,t)$. Given experimental data for diffusion of one component in one dimension, one could determine the diffusion coefficients a follows. [13]

Assume an experiment with initially a known concentration of a component on the left side and zero concentration of that component on the right side. At the start of the experiment diffusion is allowed to occur, then after a known period of time the diffusion process is halted, and the ending concentration is measured at various positions, so that $C$ is known at time $t_{end}$ for each $x$. Using the substitution described in section 2.1 of $\lambda = x/\sqrt{t}$ at the known time $t_{end}$, the ending concentrations can be organized in terms of $C(\lambda)$ instead. The resulting curve will then actually be valid for different combinations of $x$ and $t$ as they relate to $\lambda$; a given $\lambda$ is equivalent to multiple different combinations of $x$ and $t$.

After plotting the curve $C(\lambda)$ of concentrations vs $\lambda$s, one could numerically determine the value for the diffusion coefficient at a given concentration, say $C^*$, by Eq. 11

$$D(C^*) = -\frac{1}{2}\left(\frac{d\lambda}{dC}\right)_{C^*} \int_0^{C^*} \lambda dC. \tag{11}$$

To determine the value of the diffusion coefficient $D(C)$ at each concentration value of interest, the process would be repeated for different $C^*$ values.

### 2.2 Multicomponent One Dimensional Diffusion

For multicomponent diffusion, the single component equations must be modified to account for the flux and concentration of $n$ different components, and the diffusion coefficient becomes an interdiffusion component between different components. Using the formalism from Onsanger [4], with subscripts to indicate which component applies and assuming that the values are scaled so that the sum of the $n$ concentrations adds up to the constant 1, the equations become:

$$J_i = -\sum_{j=1}^{n-1} D_{ij} \frac{\partial C_j}{\partial x}, \tag{12}$$

$$\frac{\partial J_i}{\partial x} + \frac{\partial C_i}{\partial t} = 0, \tag{13}$$

$$\frac{\partial C_i}{\partial t} = \frac{\partial}{\partial x}(D_{ij}\frac{\partial C_j}{\partial x}), \tag{14}$$

$$\sum_{i=1}^{n} C_i = 1. \tag{15}$$

Since the $n$ concentrations sum to 1, one of the concentration values is a dependent variable of the other $n-1$ independent concentrations.

# 3 Theoretical Approach To Determining Multicomponent Interdiffusion Coefficients

An approximate solution to the diffusion coefficients can be determined if they are treated as an average value constant over a small range, and then analyze the overall system as a number of consecutive elements of small range [5].

The diffusion flux, $J_i$, satisfies Eq. 12, where $n$ is the total number of components in the system. If the flux, $J$, and $\partial C/\partial x$ could be determined independently, then one could determine the $D_{ij}$ coefficients.

The general approach requires knowledge of the concentration $C$ values of a multicomponent system at given positions at a given time (this can be obtained experimentally), along with the ability to determine the $\partial C/\partial x$ based on the values of $C$, and the ability to calcuate $J$. The global position range from $x_L$ to $x_R$ is divided into small elements and analyzed separately, but requiring that the concentration and first derivative of concentration match at the node edges between each element. This is known as $C_1$ continuity [6].

Given the concentration $C$ values, cubic Hermite interpolation, which utilizes both $C$ and $\partial C/\partial x$ values at end nodes, is used to best fit a curve to the experimental data, determining $\partial C/\partial x$ values at each node for the best fit.

Then knowing $\partial C/\partial x$ values, Eq. 16

$$J(x) = \frac{1}{2t}\int_{x_L}^{x}(x' - x'_M)(\frac{dC}{dx})dx', \tag{16}$$

is used to calculate $J$ (where $t$ is the time, $x_L$ is the lower limit of the range of $x$ positions in the experiment, $x$ is the position of interest, and $x_M$ is the location of the Matano plane).

For the purpose of this report, the number of components, $n$, in the system is assumed to be 3, and since by Eq. 15 they sum to 1, determinations need to be made for $n-1=2$ component concentrations and the last component concentration is implied.

Expanding Eq. 12 results in the following (where $\bar{D_{ij}}$ is the average value of $D_{ij}$ in the range from $x_1$ to $x_2$):

$$\int_{x_1}^{x_2} J_1 dx = -\bar{D_{11}}\int_{C_1(x_1)}^{C_1(x_2)} dC_1 - \bar{D_{12}}\int_{C_2(x_1)}^{C_2(x_2)} dC_2, \tag{17}$$

$$\int_{x_1}^{x_2} J_2 dx = -\bar{D_{21}}\int_{C_1(x_1)}^{C_1(x_2)} dC_1 - \bar{D_{22}}\int_{C_2(x_1)}^{C_2(x_2)} dC_2. \tag{18}$$

Equations 17 and 18 can then be evaluated to 19 and 20

$$\bar{D_{11}}(C_1(x_1) - C_1(x_2)) + \bar{D_{12}}(C_2(x_1) - C_2(x_2)) = \int_{x_1}^{x_2} J_1 dx, \tag{19}$$

$$\bar{D_{21}}(C_1(x_1) - C_1(x_2)) + \bar{D_{22}}(C_2(x_1) - C_2(x_2)) = \int_{x_1}^{x_2} J_2 dx. \tag{20}$$

The $C$ values are known from the experimental data, and $J$ values are calculated using Eq. 16. This yields two equations but four $\bar{D}$ unknowns. To overcome this, two additional equations are generated using the method of moments [8] [9] [10] [11], multiplying both sides of 17 and 18 by $(x - x_M)$ inside the integral [note $x_M$ is the position of the Matano plane].

$$\int_{x_1}^{x_2}(x - x_M)J_1 dx = -\bar{D_{11}}\int_{C_1(x_1)}^{C_1(x_2)}(x - x_M)dC_1 - \bar{D_{12}}\int_{C_2(x_1)}^{C_2(x_2)}(x - x_M)dC_2, \tag{21}$$

$$\int_{x_1}^{x_2}(x-x_M)J_2dx = -\bar{D_{21}}\int_{C_1(x_1)}^{C_1(x_2)}(x-x_M)dC_1 - \bar{D_{22}}\int_{C_2(x_1)}^{C_2(x_2)}(x-x_M)dC_2. \quad (22)$$

Using Eq. 16, equations 21 and 22 can be evaluated to 23 and 24

$$\bar{D_{11}}(2t)(J_1(x_1)-J_1(x_2)) + \bar{D_{21}}(2t)(J_2(x_1)-J_2(x_2)) = \int_{x_1}^{x_2}(x-x_M)J_1(x)dx, \quad (23)$$

$$\bar{D_{21}}(2t)(J_1(x_1)-J_1(x_2)) + \bar{D_{22}}(2t)(J_2(x_1)-J_2(x_2)) = \int_{x_1}^{x_2}(x-x_M)J_2(x)dx. \quad (24)$$

### 3.1 Approach To Calculate Interdiffusion Coefficients

To summarize the approach, given experimental data for concentrations $C$ at known positions at a known time,

1. Finite element techniques are used to split the overall position range into small elements (each end of an element is known as a node)
2. Cubic Hermite interpolation curves are used to best fit the experimental concentration data within an element to determine derivatives of Concentrations $\partial C_i/\partial x$ at each node
3. Equation 16 is used to calculate the fluxes $J_i$ as needed
4. The average values for interdiffusion coefficients $D_{ij}$ are calculated using
   - equations 19 and 23 for $D_{11}$ and $D_{12}$
   - equations 20 and 24 for $D_{21}$ and $D_{22}$

The next section describes the practical application of this approach with a set of experimental data to determine the interdiffusion coefficients.

# 4 Practical Application and Multicomponent Interdiffusion Coefficient Results

One of the dependencies in the approach described in Section 3 is knowledge of $\partial C_i/\partial x$. Given experimental data for the concentrations of a component at several positions, a cubic Hermite interpolation function can be fit to map to the data. This interpolation (Eq. 25) assumes that at two end nodes the value of the function is known as well as the value of the first derivative of the function [6]

$$f(\xi) = f_1 N_1(\xi) + (\frac{df}{d\xi})_1 \bar{N}_1(\xi) + f_2 N_2(\xi) + (\frac{df}{d\xi})_2 \bar{N}_2(\xi). \tag{25}$$

In this equation, $f$ is the function being interpolated ($C_i$ in this project), and $N_i$ are the various interpolation polynomials, shown in equations 26, 27, 28, and 29.

$$N_1(\xi) = (2 - 3\xi + \xi^3)/4, \tag{26}$$

$$\bar{N}_1(\xi) = (1 - \xi - \xi^2 + \xi^3)/4, \tag{27}$$

$$N_2(\xi) = (2 + 3\xi - \xi^3)/4, \tag{28}$$

$$\bar{N}_2(\xi) = (-1 - \xi + \xi^2 + \xi^3)/4. \tag{29}$$

Instead of knowing the function and its derivative at each node and interpolating to find a value for the function at a given location, the situation is slightly reversed. In this case, the function values are known at a large number of positions and we know the interpolation shape functions to apply at a given node, but at a node only know the function value and not its derivative. However, since we know the function value at positions between nodes, we

know what the interpolation result should be at those positions. Instead of using the cubic Hermite interpolation to determine function values at arbitrary locations, we can fit the curve of the cubic Hermite interpolation to best fit the known function values between nodes by varying the assumed function derivatives at the nodes. Once this is accomplished and $\partial C_i/\partial x$ is known, we can then apply the equations in Section 3 to determine the interdiffusion coefficients $D_{ij}$.

The entire global range of positions from the experimental data is split into smaller elements, with a node at each end. $\xi$ is the position in local coordinates, ranging from $-1$ to 1 within a given element. Since the experimental positions are originally measured "globally" (using the $x$ coordinate) from the beginning of the measured region ($x_L$) to the end ($x_R$), this will require the coordinates to be converted from one coordinate system to the other. The equations for doing this follow.

$$x(\xi) = \frac{a+b}{2} + \frac{b-a}{2}\xi, \tag{30}$$

$$\xi(x) = \frac{2x-a-b}{b-a}, \tag{31}$$

$$\frac{dx}{d\xi} = \frac{b-a}{2}, \tag{32}$$

$$\frac{d\xi}{dx} = \frac{2}{b-a}. \tag{33}$$

Here, $x$ is the global coordinate, $\xi$ is the local coordinate, and $a$ and $b$ are the lower and upper limits of the element (the end nodes) in global coordinates.

Experimental data was obtained from a diffusion experiment involving annealing two alloys at 775° C for 2 days and specifying the concentrations of three metals (Copper, Zinc, and Nickel) at x positions from 0 to 500 um [14] [5].

Implementing Step 1 and Step 2 of the approach, the global position range was broken into different elements with a number of experimental data points between each pair of nodes, and a cubic Hermite interpolation function curve for each component metal was best fit to the data incrementally element by element with the right side node in one element

becoming the left side node in the next, resulting in an estimated value for $\partial C_i/\partial x$ at each node.

Figure 2 shows the experimental data as well as the interpolated concentration curves generated using the estimated $\partial C_i/\partial x$ at each node.

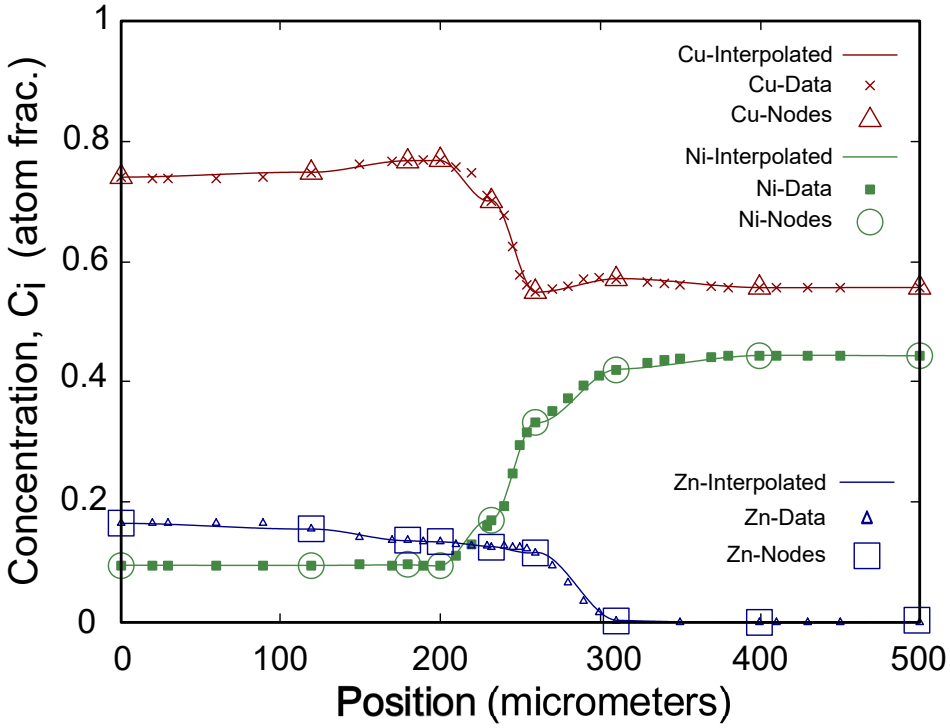


Figure 2: Experimental data and Interpolated concentration curves using calculated derivatives at nodes are shown.

At this point, the position, concentration, and concentration derivative for each node for each of the three metal types is known (the types were assigned as 1 - Copper, 2 - Nickel, 3 - Zinc).

Given the nodal values for position and concentration from the experiment and now the concentration derivatives from steps 1 and 2, the interdiffusion coefficients can be determined following steps 3 and 4 described in Section 3.

Simulations were performed to calculate the interdiffusion coefficients as the $\bar{D}_{ij}$ average value within an $x_1$ to $x_2$ range with those positions specified as input. Within each pair of positions, the simulation implemented the equations and performed the integrations

necessary to establish the equations described in Section 3 and then solved for $\bar{D}_{ij}$.

The interdiffusion coefficients are a function of the concentrations, although $\bar{D}_{ij}$ is treated as a constant average value in small regions. Figure 3 shows how the coefficients vary with position.

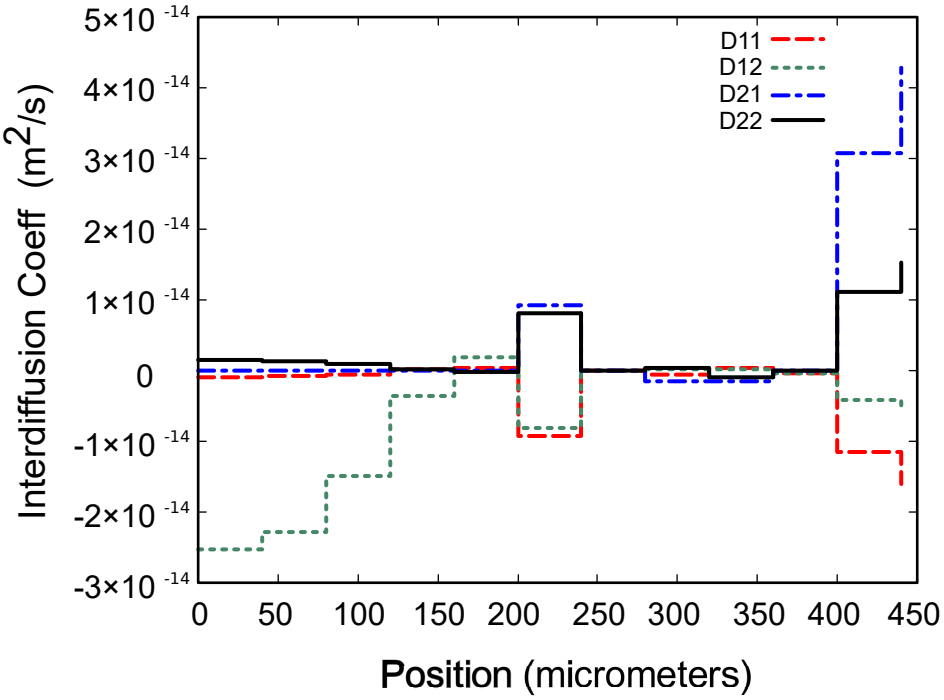


Figure 3: Interdiffusion coefficients variation with position is shown.

The interdiffusion coefficients were then examined in two broad sections, to the left of the Matano plane and to the right of the Matano plane. The average D coefficients are shown in Table 1.

Table 1: Average Interdiffusion Coefficients $\bar{D}_{ij}^{(3)}$

| Range of regions, $\mu$m | $\bar{D}_{11}, \mathrm{m}^2/\mathrm{s}$ | $\bar{D}_{12}, \mathrm{m}^2/\mathrm{s}$ | $\bar{D}_{21}, \mathrm{m}^2/\mathrm{s}$ | $\bar{D}_{22}, \mathrm{m}^2/\mathrm{s}$ |
|---|---|---|---|---|
| 0, 250 | 7.51E-16 | 5.77E-16 | 1.44E-16 | 1.15E-16 |
| 250, 500 | -2.23E-16 | -4.80E-17 | -3.28E-15 | -7.27E-16 |

The values shown in Table 1 were calculated using 9 nodes (8 elements) from the global left to global right position.

The calculations were repeated using a different number of nodes for the cubic her-

mite best fit interpolation, ranging from 4 to 9 (so 3 to 8 elements), and we expect the results to be more accurate with a higher number of nodes. With just a few nodes, the addition of another node has a large impact on the calculations but once a sufficient number of nodes is reached the calculated results converge. This can be seen in Figure 4 and Figure 5 with large variations on the left but small variation in the results between using 8 and 9 nodes (7 and 8 elements).

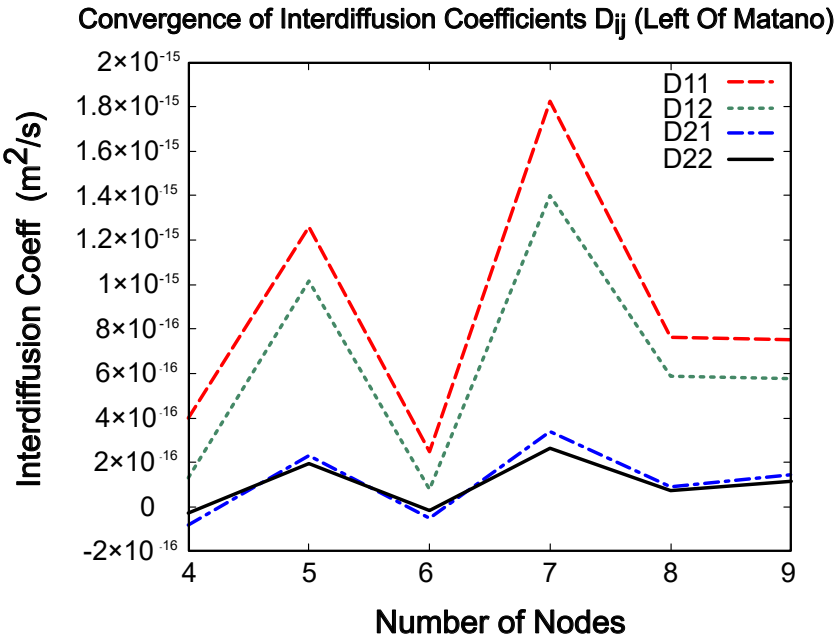


Figure 4: Convergence of Interdiffusion Coefficients as Number of Nodes Increases is shown.

## 5 Time Evolution Theoretical Approach

Knowing the interdiffusion coefficients and concentrations for a spatial region, one can also analyze the overall system as it evolves through time. Eq. 34 describes the diffusion system, incorporating time.

$$\frac{\partial C_i(x,t)}{\partial t} = \partial_x D_{ij} \partial_x C_j(x,t). \tag{34}$$

One can separate out the space and time aspects of the concentration with a represen-

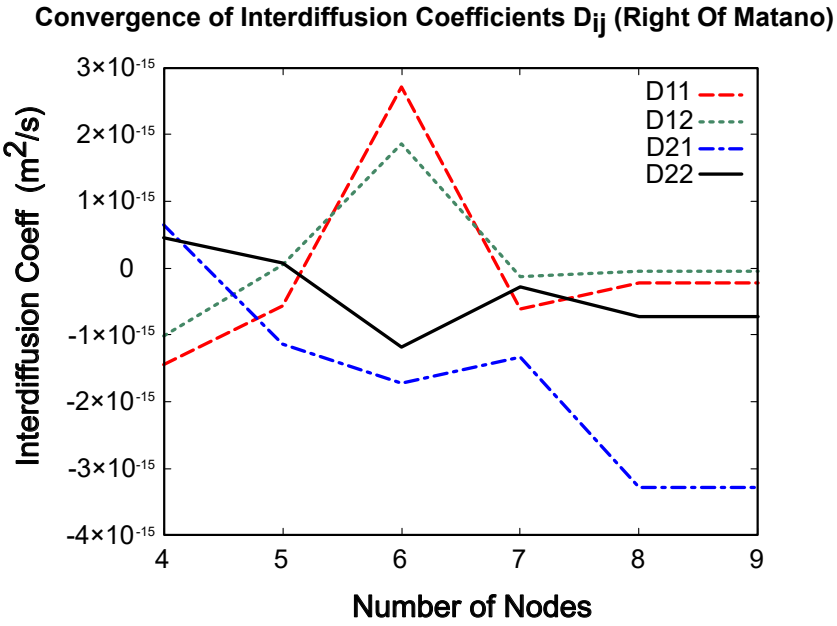


Figure 5: Convergence of Interdiffusion Coefficients as Number of Nodes Increases is shown.

tation of the concentration as shown in Eq. 35 where $C_\alpha(t)$ accounts for the concentration evolving over time and $N_\alpha(x)$ (a shape function) accounts for concentration varying with position

$$C(x,t) = \sum_\alpha C_\alpha(t) N_\alpha(x). \tag{35}$$

Here the degree of freedom at each node corresponds to the concentration and derivative of concentration.

Applying Eq. 35 to Eq. 34 results in

$$\frac{\partial}{\partial t}\left[\sum_\beta C_i^\beta(t) N_\beta(x)\right] = \partial_x D_{ij} \partial_x \sum_\gamma C_j^\gamma(t) N_\gamma(x) \tag{36}$$

Using a Galerkin approach as in standard Finite Element Method analysis and multiplying both sides by a shape function and integrating over $x$ results in

$$\int dx N_\lambda(x) \frac{\partial}{\partial t} \sum_\beta C_i^\beta(t) N_\beta(x) = \int dx N_\lambda(x) \frac{\partial}{\partial x} D_{ij} \frac{\partial}{\partial x} \sum_\gamma C_j^\gamma(t) N_\gamma(x). \tag{37}$$

$D_{ij}$'s are assumed known and constants within small sections or elements (as calcu-

lated in the previous section); rearranging Eq. 37 to

$$\int dx N_\lambda(x) N_\beta(x) \dot{C_i^\beta}(t) = D_{ij} \int dx N_\lambda(x) \frac{\partial}{\partial x} \frac{\partial}{\partial x} N_\gamma(x) C_j^\gamma(t). \tag{38}$$

Putting it into the matrix form

$$\mathbf{A} \cdot \dot{\mathbf{C}}_\mathbf{i}^\beta(t) = \mathbf{K} \cdot \mathbf{C}_\mathbf{j}^\gamma(t), \tag{39}$$

with

$$\mathbf{A} = \int dx N_\lambda(x) N_\beta(x), \tag{40}$$

and integrating the right hand side of Eq. 38 by parts yields

$$\mathbf{K} = -D_{ij} \int dx \frac{\partial}{\partial x} N_\lambda(x) \frac{\partial}{\partial x} N_\gamma(x). \tag{41}$$

Finally, invert $\mathbf{A}$ and multiply both sides of Eq. 39 to obtain

$$\dot{\mathbf{C}}_\mathbf{i}^\beta(t) = (\mathbf{A}_{\beta\lambda}^{-\mathbf{1}} \mathbf{K}_{\lambda\gamma}) \mathbf{C}_\mathbf{j}^\gamma(t), \tag{42}$$

or

$$\dot{\mathbf{C}}_\mathbf{i}^\beta(t) = \mathbf{M} \cdot \mathbf{C}_\mathbf{j}^\gamma(t). \tag{43}$$

The solution to Eq. 43 describes how the concentration evolves through time. It takes the general form of

$$\mathbf{C}(x,t) = \mathbf{exp}(\mathbf{M}t) \cdot \mathbf{C}(x, t=0) \tag{44}$$

where

$$\mathbf{M} = \mathbf{A}_{\beta\lambda}^{-\mathbf{1}} \mathbf{K}_{\lambda\gamma}. \tag{45}$$

The next section describes the practical application of this approach with a set of experimental data and the interdiffusion coefficients determined earlier to then time evolve

the concentration of the metals forward from their initial state at time 0.

## 6 Time Evolution Practical Application and Results

Simulations were performed to solve the equations described in Section 5 and assemble the **A** and **K** matrices. **M** was then found by taking the inverse of **A** and multiplying by **K**. Knowing **M**, the equation 44 was implemented to find the concentration values as the system evolves through time. The time ranged from 0 to 48 hours, or two days.

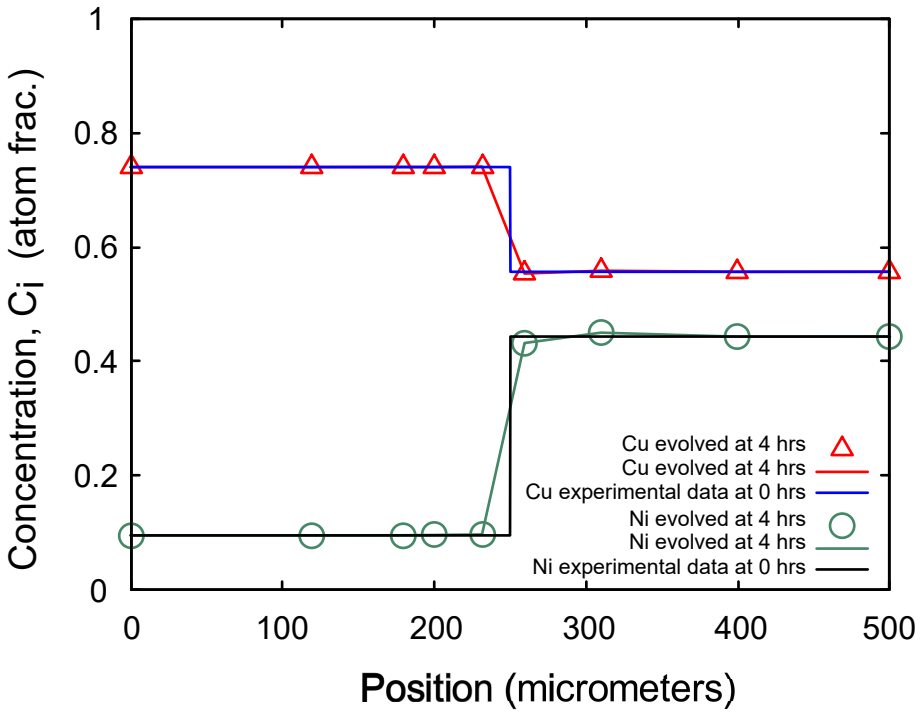


Figure 6: Time Evolution to 4 Hours is shown.

In Figure 6, the time-evolved concentrations after 4 hours for Cu and Ni are compared to the initial experimental values for the concentrations at $t_0$. The initial experimental data resembles a step function, showing constant values to the left and right of the junction between the metals at $250\mu m$, and a vertical discontinuity at the junction, showing an abrupt change between the bars. The time-evolved data is represented by shapes (triangles or circles) at the nodes and dashed lines between them. The time-evolved data is beginning to vary slightly from the original concentration values because the metals are starting to

diffuse.

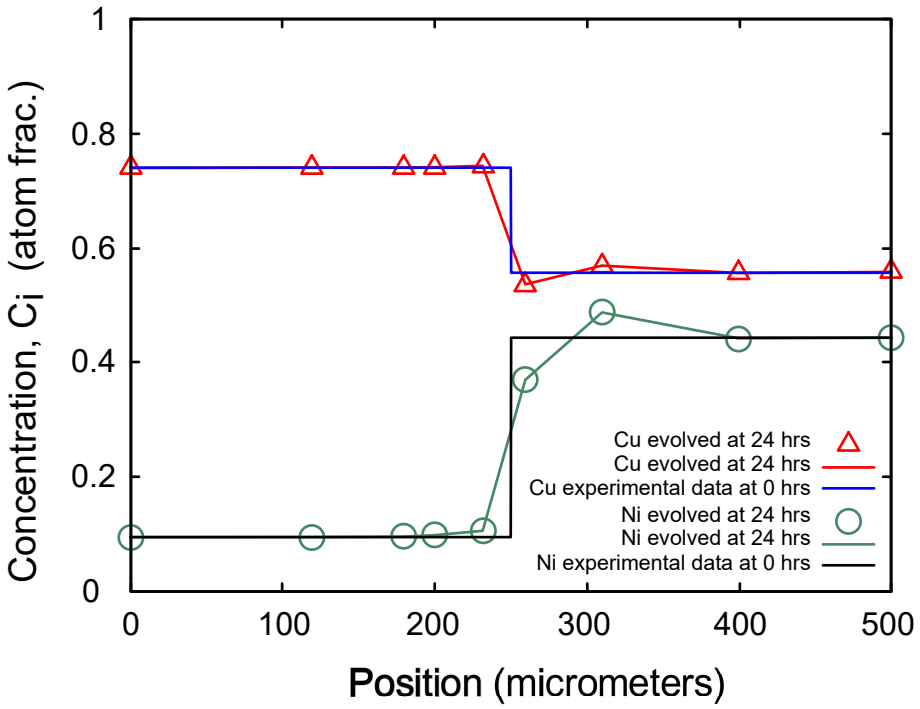


Figure 7: Time Evolution to 24 Hours is shown.

In Figure 7, after 24 hours, the metals are continuing to diffuse. The concentrations for the two metals are deviating more from the initial conditions.

In Figure 8, the time-evolved data at 48 hours is compared to the experimental concentrations at 48 hours. The experimental data is represented by squares for copper and 'X's for nickel, and the time-evolved data is represented by triangles for copper and circles for nickel. After 48 hours, the results have some error compared to the experimental data, but the general shapes agree.

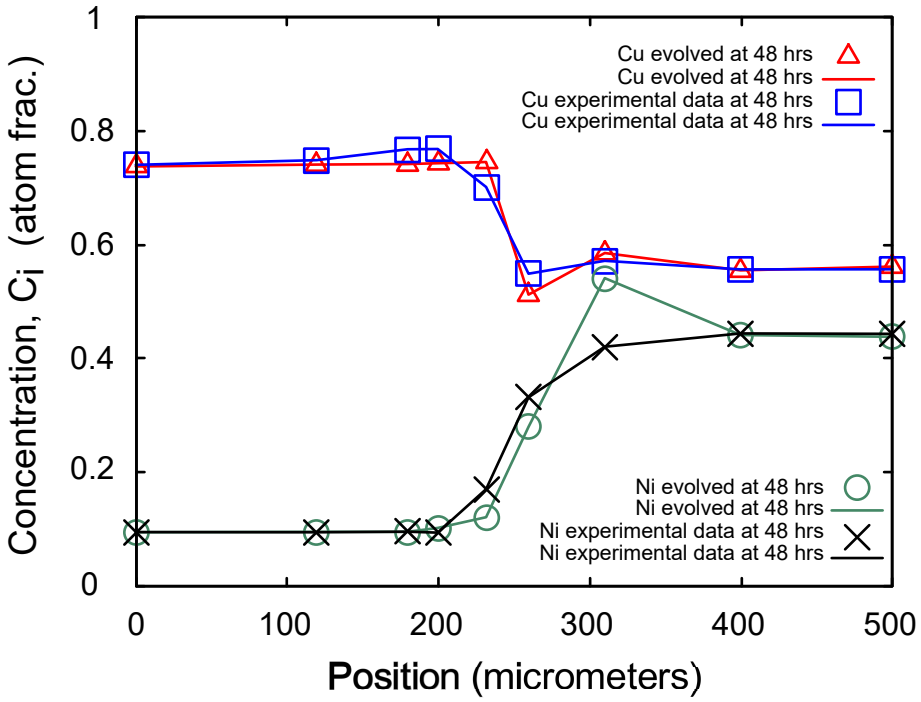


Figure 8: Time Evolution to 48 Hours vs Experiment Data at 48 Hours is shown.

# 7 Avoiding Interdiffusion D Coefficient Calculations

The prior approach used moment analysis [11] to calculate interdiffusion coefficients and then use them in the calculation of a matrix to time evolve the concentrations.

It may be possible to establish a time evolution equation in a different way which bypasses the need to determine interdiffusion coefficients with more use of the equation of continuity,

$$\frac{\partial C_i(x,t)}{\partial t} + \frac{\partial J_i(x,t)}{\partial x} = 0. \tag{46}$$

The details are presented in subsection 7.1.

## 7.1 Theoretical Considerations

Starting with Boltzmann scaling for the diffusion equation, and asserting [12] that the scaled variable is $\lambda = x/\sqrt{t} = x * t^{-\frac{1}{2}}$, leads to

$$\frac{\partial J_i(x,t)}{\partial x} = \frac{(x - x_0)}{2(t - t_0)} \frac{\partial C_i(x,t)}{\partial x}. \tag{47}$$

Here $x_0$ refers to the location of the Matano plane in the laboratory coordinates, and $t$ is the diffusion time while $t_0$ is the time at which diffusion begins. The $\frac{1}{2}$ factor in Eq. 47 is due to the time exponent in the Boltzmann scaling expression. In general, if $\lambda = x \cdot t^{-\nu}$, then the factor in Eq. 47 would be $\nu$.

The flux $J_i(x,t)$, could be determined from the experimental measured concentrations via its gradient using

$$\begin{aligned} J(x,t) - J(x_{\text{left}},t) \;\; &= \\ &\frac{1}{2(t - t_0)} \int_{x_{\text{left}}}^{x} dx \; (x - x_0) \frac{\partial C_i(x,t)}{\partial x}. \end{aligned} \tag{48}$$

As before, the range of the diffusion can be divided into a number of small finite elements and then experimental concentration data can be fit using cubic Hermite inter-

polation polynomials as described in Section 4 to determine the values of the derivative of concentration $C'$. With the value for $C$ and $C'$ determined, the concentration can then be interpolated within an element using Eq. 35 and in more general terms in Eq. 49

$$C(x,t) = \sum_{\alpha}^{ndof} C_\alpha(t) N_\alpha(x) \tag{49}$$

where the nodal degrees of freedom ($ndof$) in each element is the number of the concentrations and their derivatives.

A finite element approach to solving Eq. (47) by the well-known Galerkin method leads to the equations

$$\begin{aligned} &\int dx \Big( N_\alpha(x) N'_\beta(x) \Big) J_\beta(t) \\ &\qquad = \frac{1}{2(t-t_0)} \int dx \Big( (x-x_0) N_\alpha(x) N'_\gamma(x) \Big) C_\gamma(t). \end{aligned} \tag{50}$$

Using a matrix notation where $M = \int dx \Big( N_\alpha(x) N'_\beta(x) \Big)$ and $B = \int dx \Big( (x-x_0) N_\alpha(x) N'_\gamma(x) \Big)$, this becomes

$$M_{\alpha\beta} J_\beta(t) \;\; = \;\; \frac{1}{2(t-t_0)} B_{\alpha\gamma} C_\gamma(t),$$

(where the subscripts indicate nodal values) or, more compactly,

$$\mathbf{J}(t) \;\; = \;\; \frac{1}{2(t-t_0)} \mathbf{M}^{-1} \mathbf{B} \cdot \mathbf{C}(t). \tag{51}$$

Here $\{\mathbf{C}, \mathbf{J}\}$ are vector arrays of the nodal values for the concentration and the flux. Assuming cubic Hermite interpolation as before, the arrays correspond to function value followed by the derivative of the function at each node. This equation provides a relation between the flux $J$ and its derivative and the concentration and its derivative at each node. Inverting the matrix M allow us to solve for the flux and its derivative at each node if $\mathbf{C}$(t) was known.

Note that the above derivation assumes that Boltzmann scaling relation holds so

that the diffusion partial differential equation reduces to a regular differential equation in a single variable $\lambda = x/\sqrt{t}$ (or $\lambda = xt^{-\nu}$).

The time evolution of the flux can also be obtained directly by solving the equation of continuity, Eq.(46) using the Galerkin method. We have

$$\int dx\Big(N_\alpha(x)N'_\beta(x)\Big)J_\beta(t) + \int dx\Big(N_\alpha(x)N_\gamma(x)\Big)\dot{C}_\gamma(t) = 0, \tag{52}$$

and using matrix notation with $M = \int dx\Big(N_\alpha(x)N'_\beta(x)\Big)$ as before and $Q = \int dx\Big(N_\alpha(x)N_\gamma(x)\Big)$ leads to

$$M_{\alpha\beta}J_\beta(t) = -Q_{\alpha\gamma}\dot{C}(t)_\gamma. \tag{53}$$

Note that $\dot{C}$ is used for $\partial C_\gamma(t)/\partial t$ . The time evolution of $C$ is given by solving the relation

$$\dot{\mathbf{C}}(t) = -\mathbf{Q}^{-1}\mathbf{M}\mathbf{J}(t). \tag{54}$$

Conversely, the flux $\mathbf{J}$(t) could be determined by Eq 55 if $\dot{\mathbf{C}}(t)$ were known.

$$\mathbf{J}(t) = -\mathbf{M}^{-1}\mathbf{Q}\dot{\mathbf{C}}(t). \tag{55}$$

The solution of the time dependence of the concentration obtained by direct integration is

$$\mathbf{C}(t) - \mathbf{C}(t_0) = -\Big[\mathbf{Q}^{-1}\mathbf{M}\Big] \cdot \int_{t_0}^{t} dt'\mathbf{J}(t'). \tag{56}$$

J would have to be determined independently. This could be done directly from experimental data without invoking scaling. Alternately, by using Boltzmann scaling we can obtain it from Eq.(48) from the experimental concentration curves.

Returning to the time evolution equation of Eq. 54, substitute Eq. 51 for $\mathbf{J}$(t)

yielding

$$\dot{\mathbf{C}} = -\frac{1}{2(t-t_0)}\mathbf{Q}^{-1}\mathbf{B}\mathbf{C}. \tag{57}$$

Letting

$$\mathbf{R} = \frac{1}{2}\mathbf{Q}^{-1}\mathbf{B}, \tag{58}$$

leads to

$$\dot{\mathbf{C}} = -\frac{1}{(t-t_0)}\mathbf{R}\mathbf{C}. \tag{59}$$

In order to develop the general matrix solution, consider just one element in the array of the vectors and collapse the matrix $\mathbf{R}$ into a single value $r$, so that

$$\frac{dC}{C} = -r\frac{dt}{(t-t_0)}, \tag{60}$$

leading to a solution

$$C(t) = \frac{1}{(t-t_0)^r}C(t_0). \tag{61}$$

This solution can be readily verified by substituting it back into the differential equation 60. Generalizing to all the components, yields

$$\mathbf{C}(t) = \left[(t-t_0)^{-\mathbf{R}}\right] \cdot \mathbf{C}(t_0). \tag{62}$$

Verify by taking the time derivative of both sides, resulting in:

$$\frac{d\mathbf{C}(t)}{dt} = \left( -\mathbf{R}dt\frac{1}{t-t_0}\right)\left[(t-t_0)^{-\mathbf{R}}C(t_0)\right], \tag{63}$$

or

$$\dot{\mathbf{C}}(t) = -\frac{1}{(t-t_0)}\mathbf{R}\mathbf{C}(t), \tag{64}$$

consistent with Eq. 59 as anticipated.

For the time evolution of concentrations as described by Eq. 62, instead of calculating

the term $(t-t_0)^{-\mathbf{R}}$, we can transform it to a matrix exponentiation. Let

$$\mathbf{T} = (t-t_0)^{-\mathbf{R}}, \tag{65}$$

and then exponentiate the natural log to get

$$\mathbf{T} = \exp\Big[\ln(t-t_0)^{-\mathbf{R}}\Big] = \exp\Big[-\mathbf{R}\ln(t-t_0)\Big]. \tag{66}$$

Substituting for $\mathbf{T}$ back into Eq. 62, a new equation for the time evolution of concentration using matrix exponentiation is obtained

$$\mathbf{C}(t) = \Big[\exp(-\mathbf{R}\ln(t-t_0)])\Big] \cdot \mathbf{C}(t_0). \tag{67}$$

Comparing to Eq. 44 from before, this one was derived without any reference to interdiffusion coefficients.

Once $\mathbf{C}$(t) is determined, $\dot{\mathbf{C}}(t)$ could be determined by Eq. 64, and then Eq. 55 could be used to determine $\mathbf{J}(t)$.

### 7.2 Application of Alternate Time Evolution Approach

Simulations were performed to solve the equations in Section 7.1, and assemble the matrices $\mathbf{Q}$ and $\mathbf{B}$, after which the matrix $\mathbf{R}$ was constructed, and Eq. 67 was implemented using matrix exponentiation. The simulation evolved this equation through times from 0 to 48 hours.

Recall that in Eq. 58, the scaling factor of $\frac{1}{2}$ was due to the time exponent in $\lambda = xt^{-1/2}$. If we let $\nu$ be the exponent (so $\lambda = xt^{-\nu}$), we can rewrite Eq. 58 as

$$\mathbf{R} = \nu\mathbf{Q}^{-1}\mathbf{B}. \tag{68}$$

The calculations were run with an initial value of $\frac{1}{2}$, or 0.5 for $\nu$ (the Boltzmann value). The

48-hour time-evolved concentration values were not accurate with this value; they converged to an incorrect, fairly constant value. Then, $\nu$ was varied in a range from 0.6 down to 0.05 to determine a value that would give more accurate results that better matched the experimental data.

*The time-evolved concentration values became more consistent with the experimental values at $\nu = 0.1$ and below, with a good fit at 0.05.*

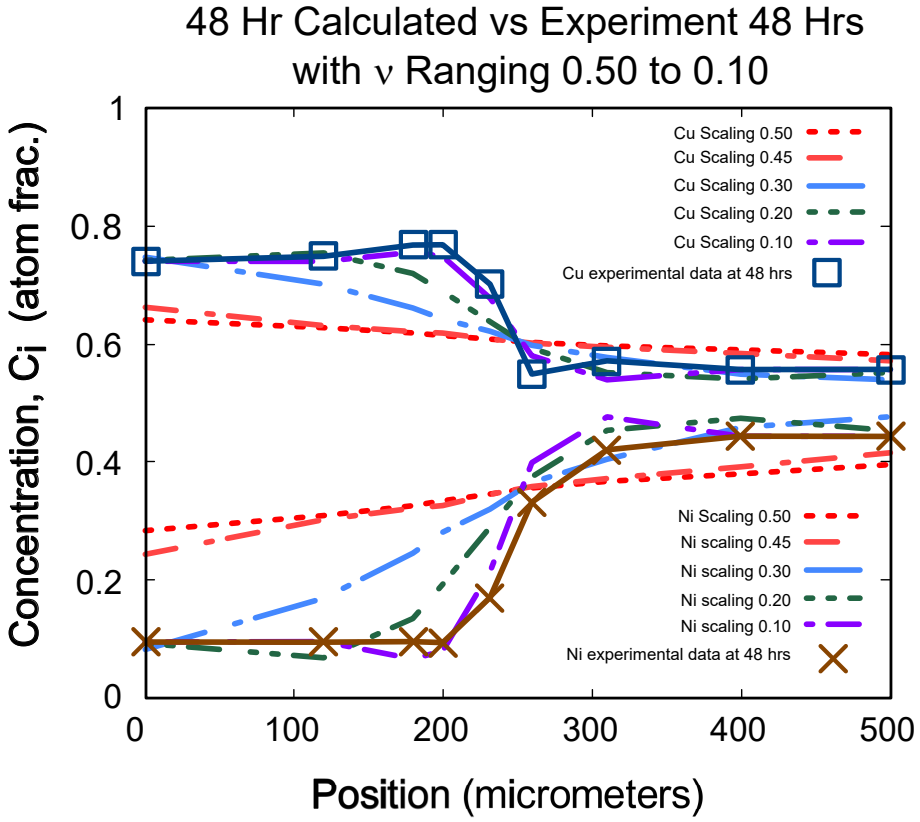


Figure 9: 48 Hour Time Evolution vs Experiment Data with $\nu$ ranging from 0.5 to 0.10 is shown.

Figure 9 displays the time-evolved concentrations at 48 hours (represented by dashed lines) compared to the experimental values at 48 hours (represented by squares and 'X's). The time-evolved concentrations shown in this figure used $\nu$ factors of $0.5, 0.45, 0.3, 0.2$, and 0.1. The calculated data is very inaccurate at $\nu = 0.5$ and progressively becomes more consistent with the experimental data as $\nu$ decreases.

Figure 10 shows the time-evolved curves for $\nu$ at 0.1 and 0.05, compared to the experimental data. The two curves are similar to each other, meaning that either value of $\nu$

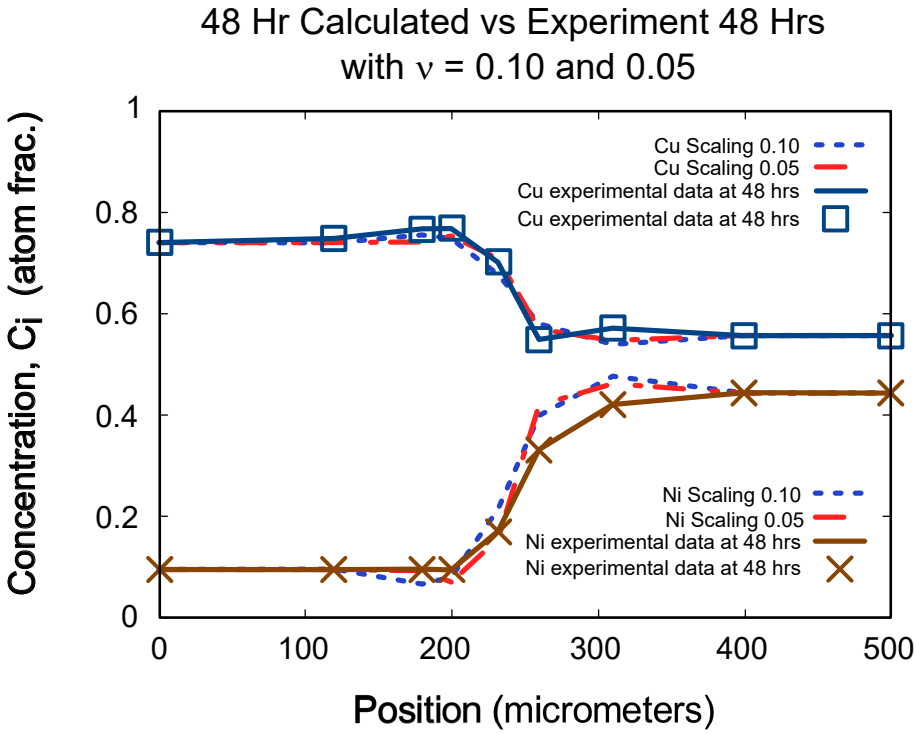


Figure 10: 48 Hour Time Evolution vs Experiment Data with $\nu$ set to 0.10 and 0.05 is shown.

can be used in calculations and still remain reasonably accurate. The time-evolved curves fit the experimental data much better in this range of $\nu$ values than at $\nu = 0.5$. In the following figures, a $\nu$ value of 0.05 was used for the calculated data.

The concentration values were time-evolved using Equation 67 with results shown at times 4 hours, 24 hours, and 48 hours, as before, and compared to the experimental concentration values. The time evolution at 4 and 24 is compared to the initial experimental data at $t_0$, and the time evolution at 48 hours is compared to the final experimental values at 48 hours.

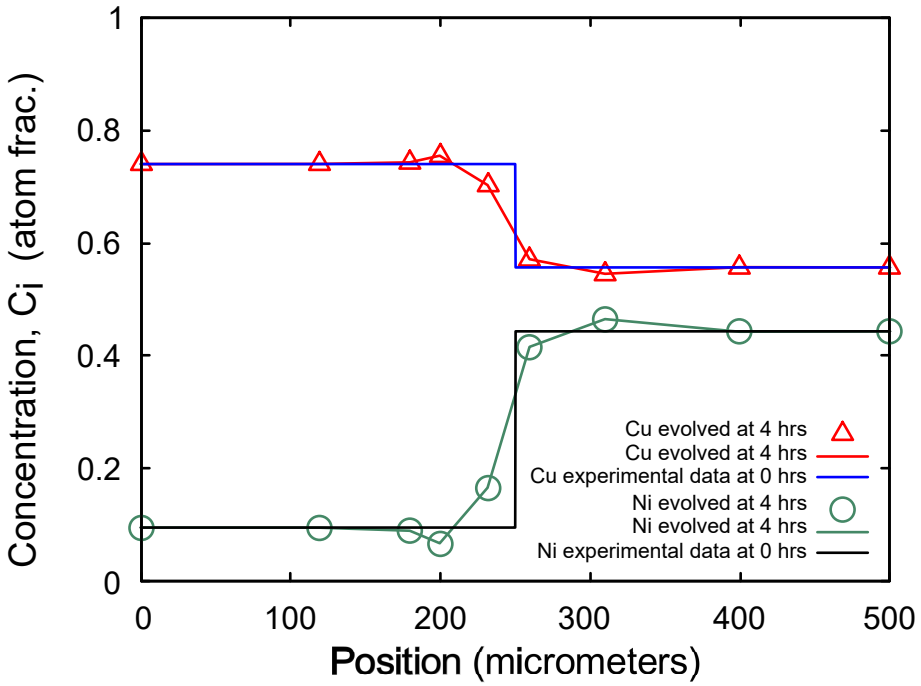


Figure 11: Time Evolution to 4 Hours is shown.

Figure 11 shows the time-evolved data (represented by dashed lines and shapes) compared to the initial experimental data for the concentrations at $t_0$ (represented by solid lines). As before, initially there is a sharp discontinuity at the junction between the two bars. The time-evolved data is evolved after 4 hours and displays some deviation from the original as the metals start to diffuse.

Figure 12 shows the time-evolved data after 24 hours, compared to the initial experimental data. The metals continue to diffuse and deviate from the initial values.

Figure 13 compares the time-evolved data at 48 hours (represented by triangles and circles) to the experimental data at 48 hours (represented by squares and 'X's). The time-evolved data follows the general shape of the experimental data.

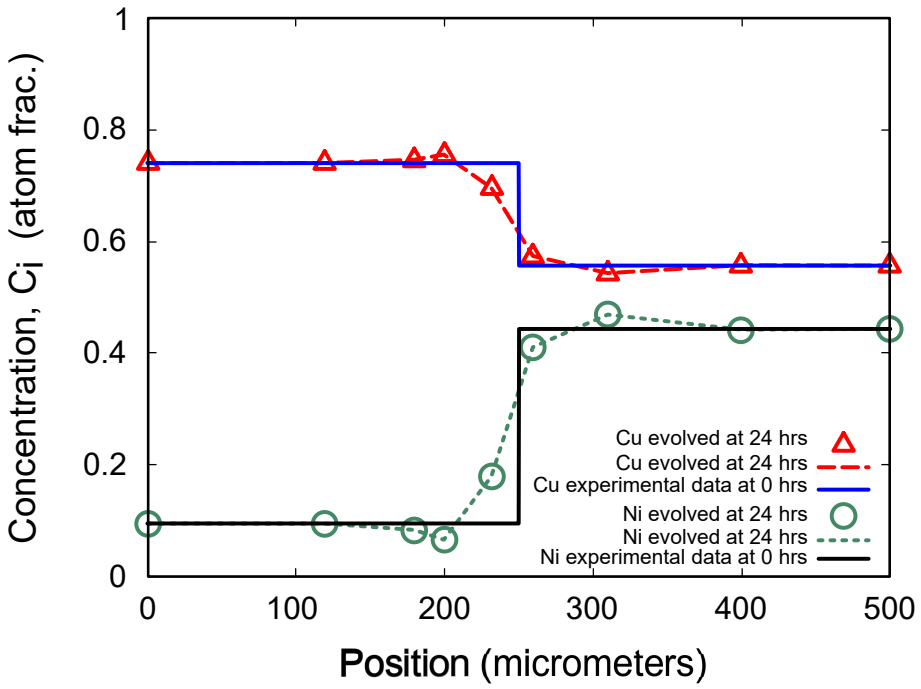


Figure 12: Time Evolution to 24 Hours is shown

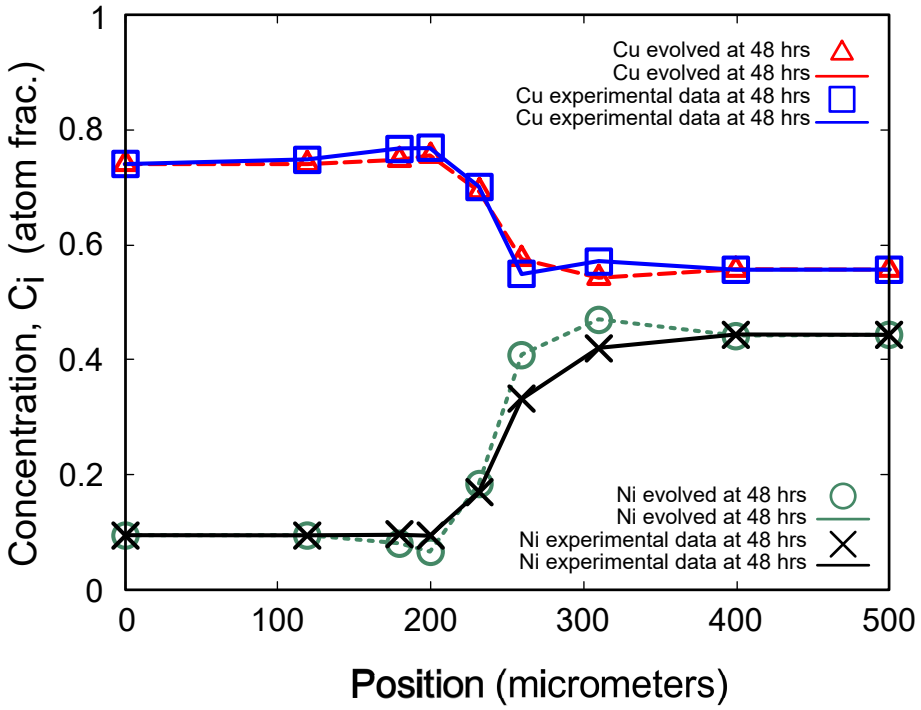


Figure 13: Time Evolution to 48 Hours vs Experiment Data at 48 Hours is shown.

Similarly accurate results can be found whether we use the interdiffusion coefficients or not; the research suggests that the new approach that bypasses the need for interdiffusion coefficients is valid.

As has been historically the case, the use of interdiffusion coefficients for multicomponent diffusion has been fraught with constraints; only the method of moments known as Dayananda analysis [8] allows one to calculate all the diffusion paths with data from a single experiment. In the new approach, the use of interdiffusion coefficients is avoided so the issue does not arise and it appears to be a novel approach. It is interesting to see that the experimental concentration curves appear to have information about the species of metals that are co-diffusing together. *There may not be a need to invoke the use of interdiffusion coefficients for multicomponent diffusion.*

## 8 Summary and Conclusions

In this project, multicomponent diffusion and the time evolution of concentrations was explored, mathematically analyzing and describing diffusion both with and without interdiffusion coefficients, and simulations were performed to implement the theory and numerically calculate results to compare with experimental data.

We started with data from a prior physical experiment which specified the concentrations of three metals (copper, nickel, zinc) at different positions after a known period of diffusion, and used finite element methods with curve fitting of cubic Hermite interpolation polynomials to determine the concentration derivatives at the element nodes.

Once the concentration values and derivatives were known at nodal positions, we proceeded to utilize a method of moments to determine the interdiffusion coefficients, which would be used in calculating the behavior of the concentration as time evolved. A matrix equation describing the time evolution of concentration at the nodes was developed.

A new approach and set of equations that bypassed the need for interdiffusion coefficients was also used, and a different equation describing the time evolution of concentration at the nodes derived.

Both methods of analysis produced results of similar accuracy to the original experimental data and the more straightforward approach which bypasses the need for an interdiffusion calculation is viable.

## 9 Acknowledgements

I would like to thank Professor L. Ramdas Ram-Mohan for his help and guidance. I would also like to thank the Center for Computational NanoScience (CCNS) and team, Debanik Das and Sathwik Bharadwaj, for their support and assistance, as well as the support of the Dean of Arts and Sciences summer research fellowships.

## References


[1] A. Fick, Ann. Phys., 1855, **170**, p. 59-86

*Uber Diffusion*

[2] L. Boltzmann, Ann Phys, 1894, **53**, 959,

*Zur Integration der Diffusiongleichung bei Variablen Diffusions-coefficienten*

[3] C. Matano, Jpn. J. Phys. (Trans.), 1933, **8**, p. 109-113

*On the Relation between the Diffusion Coefficients and Concentrations of Solid Metals (The Nickel-Copper System*

[4] L. Onsanger, Ann. NY Acad. Sci., 1945, **46**, p. 241-265

*Theories and Problems of Liquid Diffusion*

[5] L. R. Ram-Mohen and M. A. Dayananda, Journal of Phase Equilibria and Diffusion, **Vol 27**, No 6, 2006

*A Transfer-Matrix Method for Analysis of Multicomponent Diffusion with Any Number of Components*

[6] L. R. Ram-Mohan, Oxford University Press, Oxford, UK, 2002,

*Finite Element and Boundary Element Applications in Quantum Mechanics*

[7] M. A. Dayananda, Metall. Mater. Trans., 1996, **27A**, p. 2504–2509,

*Average Effective Interdiffusion Coefficients and the Matano Plane Composition*

[8] M .A. Dayananda and Y. H. Sohn, Metall. Mater. Trans., 1999, **30A**, p. 535-543,

*A New Analysis for the Determination of Ternary Interdiffusion Coefficients from a Single Diffusion Couple*

[9] M. A. Dayananda, Metall. Trans., 1983, **14A**, p 1851-1858

*An Analysis of Concentration Profiles for Fluxes, Diffusion Depths, and Zero-Flux Planes in Multicomponent Diffusion*

[10] M. A. Dayananda, J. Phase Equilib. Diffus., 2005, **26**, p. 441-446
*Analysis of Multicomponent Diffusion Couples for Interdiffusion Fluxes and Interdiffusion Coefficients*

[11] K. M. Day, L. R. Ram-Mohan, and M. A. Dayananda, Journam Phase Equilib. Diffus., 2006, **26**, p. 579-590
*Determination and Assessment of Ternary Interdiffusion Coefficients from Individual Diffusion Couples*

[12] M. A. Dayananda and C.W. Kim, *Metall Trans*, 1979, **10A**:1333
*Zero-Flux Planes and Flux Reversals in Cu-Ni-Zn Diffusion Couples*

[13] L. R. Ram-Mohan,
*Unpublished notes*

[14] M. A. Dayananda, Purdue University,
Experimental data for concentration profiles of Cu-Ni-Zn couple $\alpha_2$ vs $\alpha_7$, annealed at 775° C for 2 days

[15] L. R. Ram-Mohan, K. H. Yoo, R. L. Aggarwal. Phys Rev B, 1988, **38**:6151,
*Transfer-matrix algorithm for the calculation of the band structure of semiconductor superlattices*

[16] B. Chen, M. Lazzouni, and L.R. Ram-Mohan,Phys. Rev. B, 1992, **45**, p 1204–1212
*The Diagonal Representation for the Transfer Matrix Method for Obtaining Electronic Energy Levels in Layered Semiconductor Heterostructures*